numerical aided machine learning on Low-RCS Orbital Debris tracking with mobile radar system

1st Samarth Paliwal
Dept. of Science
University of Arizona
Tucson, United States
0009-0008-8587-1214

***Abstract*—In the review of the growing amount of satellites, orbiting space debris and other smashed debris like the Iridium-33, In the low earth orbit(LEO) rising the risk of more satellite impacts and with this increase, the astronomy observing window is also getting devoured. Thus propose to utilize ephemeris-constrained gating(SATnogs and TLEs) with FPGA-resident deep neural network inference, enhance error uncertainty. IF to an embedded stack that quantized 1D-CNN on the FPGA with SBC handles model load, keying, and scheduling for synchorization. Multistatic(raw tensors) receivers increase aspect diversity and resolution sharpness off-site. Trained gating uncertainty, characterizing latency and resource budgets for real-time throughput, and prove with experimental theories with model predictive control (MPC) overseeing the closed loop.**

***Index Terms*—LEO debris, signal processing, Machine Learning**

I. Introduction

ML detection for SO_o offload spectrograms for batch inference incurs latency and scalability by the FPGA pipeline. CNN numerically learns provided hypothesis space stated in the 2LE ephemeris models, which accelerates detectability for Low-RCS, enabling active tracking. The tight interaction among catalog priors, multi-static diversity, and FPGA-resident inference operating on slow-time/fast-time radar data under strict latency and resource constraints.

Utilizing Machine learning process with supervised convolution neural network system to study the I/Q stream log. Developing a mathematical model in defining the LEO objects projections, differentiating the radio stream flow identifying the space debris.

standalone monopole antenna array, from a distance difference. Phase controlling system, clock crystal identification,

II. System Architecture

In Fig.1, shown frequency entry to SBC(Data Compression) initializes the model to perform active parallel computing. An FPGA executes the quantized forward pass together with pre- and post-processing so that gating masks, thresholding, and classification remain within the hardware timing envelope. Candidate ephemerids are propagated via SGP4/SDP4 to produce time-tagged predictions of range, rate, and azimuth/elevation footprints. Sectioning and determining detection and classification are attempted, dramatically reducing compute and memory traffic compared to non-FPGA.

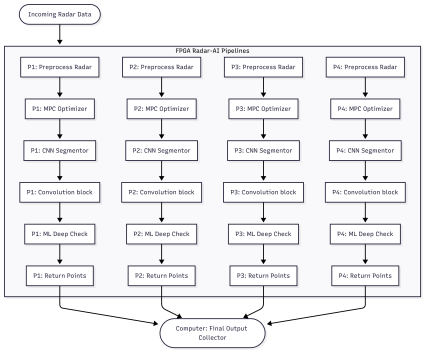

Fig. 1. Design of the FPGA Recursion

III. Catalog-Aware Gating

Let $\boldsymbol{\theta}_t$ denote the propagated state with covariance Σ_t for convolutions. Thereby, time–range–Doppler–angle window

$$\mathcal{W}_t = \left\{ (\tau, f_D, \alpha) : \left\| \boldsymbol{h}(\boldsymbol{\theta}_t) - [\tau, f_D, \alpha]^\top \right\|_{\Sigma_t^{-1}} \leq \gamma \right\},$$

$\boldsymbol{h}(\cdot)$ is the measurement model and γ is chosen by the false detection range. Calibration terms absorb ionospheric path delay, clock bias, and baseline errors. When catalog errors grow, robust gating inflates Σ_t and evaluates a small bank of nearby hypotheses to limit miss bias without exploding compute.

IV. Signal Formation and Features

Each antennas stabilizes amplitude and phase, mitigates clutter, and forms slow-time/fast-time patches around $\mathcal{W}_t$. For early experimentation, a spectrogram path accelerates iteration, while the deployment path uses compact 1D IF segments for edge efficiency. Tensors $\boldsymbol{X} \in \mathbb{R}^{T \times F}$ preserve micro-Doppler structure while minimizing bandwidth and on-chip memory.

V. FPGA-Resident Network

A pipeline-wise squeeze–excitation maps $\boldsymbol{X}$ to SO_o-vs-null logits and optional micro-Doppler attributes. Multi-convolution execution returns INT8 weights and activations aligned with DSP slices and BRAM. When additional temporal context is required, a gated 1D temporal block or tiny ConvLSTM is folded into the tail without violating timing. Inner-loop inference, gating application, and decision logic executes

on the FPGA; the SBC handles model load, telemetry, and control.

VI. Multistatic(sensor) Fusion

Synchronized stations provide aspect and bistatic diversity. A soft fusion score

$$\Lambda = \sum_{s=1}^{S} \log p_\phi(y_s = 1 \mid \boldsymbol{X}_s, \mathcal{W}_t)$$

sharpens resolution as raw tensors remain. FPGA clock tree module's sub-sample timing, track-before-detect over gated cells improves marginal-SNR performance without relaxing the false-alarm budget.

VII. Latency and Resource Model

The end-to-end budget

$$T_{\mathrm{e2e}} = T_{\mathrm{acq}} + T_{\mathrm{gate}} + T_{\mathrm{pre}} + T_{\mathrm{infer}} + T_{\mathrm{fuse}}$$

is constrained by pass dynamics. Feasibility is enforced by

$$\mathrm{D}_{\mathrm{CNN}} + \mathrm{D}_\rho \le \mathrm{D}_{\mathrm{B}},\ j_f + j_\alpha \le j_B$$

D—Dsp. f—feat. B—FPGA. α—act. ρ—pre. j—BRAM. throughput at or above the post-gating sample rate. These relations guide kernel tiling, on-chip buffering, and stream scheduling. MPC supervises thresholds and gating size in response to measured latency and SNR for error.

VIII. Training and Generalization

mixed precision(define yes no or how many), and regularizes via domain randomization over, and clutter spectra. TLE-noise augmentation teaches robustness to ephemeris errors so the network tolerates modest gating drift without catastrophic misses.

Phase 1 utilize spectrogram for separability with curated passes, synthetic injects and noise hardening. Phase 2 deploys to 1D IF patches for quantization training, regularize domain randomization over clock offset, IF shear,

IX. Evaluation Plan

We measure probability of detection at a fixed false-alarm rate versus effective RCS proxies under controlled SNR, and report end-to-end latency from acquisition to decision. An ablation study isolates the contributions of gating, fusion, and quantization. A theory component characterizes gating volumes under TLE covariance and connects window size to missed-detection probability at a given operating point. A system study compares single-station against multistatic fusion on real passes to quantify diversity gains.

X. Risks and Mitigations

Catalog inaccuracies may over-restrict search; covariance inflation and small hypothesis banks reduce miss risk. FPGA resource pressure can force model shrinkage; depthwise separable designs and INT8 quantization preserve accuracy per LUT/DSP. Synchronization and calibration threaten reproducibility; disciplined timing, calibration tones, and periodic self-checks maintain alignment.

XI. Wavelength Selection and Physical Modeling

For monostatic radar, the received power is

$$P_r = \frac{P_t G_t G_r \lambda^2 \sigma}{(4\pi)^3 R^4 L}. \tag{1}$$

In the Rayleigh region ($d \ll \lambda$) an effective RCS scales as

$$\sigma = C(m)\,\frac{d^6}{\lambda^4}, \qquad C(m) = \pi^5 \left|\frac{m^2-1}{m^2+2}\right|^2, \tag{2}$$

so combining with (1) yields $P_r \propto d^6/(\lambda^2 R^4)$ at fixed geometry and target size. Hence

$$\frac{P_r(\lambda_2)}{P_r(\lambda_1)} = \left(\frac{\lambda_1}{\lambda_2}\right)^2. \tag{3}$$

Comparing the S band $\lambda_1 \approx 10\,\mathrm{cm}$ with the C band $\lambda_2 \approx 5\,\mathrm{cm}$ gives a gain $\approx 6\,\mathrm{dB}$ for low-centimeter RCS targets in the C band, provided $d \lesssim \lambda/2\pi$ remains in the Rayleigh or near-Mie transition. This motivates the operation of the C-band for small debris, while acknowledging atmospheric and regulatory constraints.

XII. Nextstep

Knowing more accuracy and efficiency at a relative rate while tracking low-RCS SO_o at operational SNRs. We hope to integrate omnidirectional antennas array, to achieve more accurate differentiability.

Let detections be $z_k \in \mathbb{R}^m$ (e.g., image or radar measurements) with appearance embedding a_k, and let the track state be $x_k = [p_x, p_y, v_x, v_y]^\top$. 1. initial detection at t_1 to obtain (z_{t_1}, a_{t_1}) and kinematic proxies $(\hat{v}_{t_1}, \hat{\theta}_{t_1})$ from finite-difference fit. 2. requires a second detection at t_2 that passes tensor thresholds. while Kalman gate at model, it proceeds predict $\tilde{x}_{t_2|t_1} = F\tilde{x}_{t_1}$ and $\tilde{P}_{t_2|t_1} = F\tilde{P}_{t_1}F^\top + Q$. With measurement matrix H and noise R, the squared Mahalanobis innovation

$$D^2 = \big(z_{t_2} - H\tilde{x}_{t_2|t_1}\big)^\top S^{-1} \big(z_{t_2} - H\tilde{x}_{t_2|t_1}\big), \qquad S = H\tilde{P}_{t_2|t_1}H^\top + R, \tag{4}$$

must satisfy $D^2 \le \chi^2_{\alpha,m}$. Passing all gates confirms the track and initializes (x_{t_2}, P_{t_2}).

Thereafter, on each scan $k = t_3, t_4, \ldots$, predict

$$x_{k|k-1} = Fx_{k-1}, \qquad P_{k|k-1} = FP_{k-1}F^\top + Q, \tag{5}$$

associate measurements using a joint gate and composite cost

$$D_k^2 = \big(z_k - Hx_{k|k-1}\big)^\top S_k^{-1} \big(z_k - Hx_{k|k-1}\big), \quad S_k = HP_{k|k-1}H^\top + R, \tag{6}$$

with $D_k^2 \le \gamma$ and $d_{\mathrm{app}} \le T_{\mathrm{app}}$; use nearest neighbor to update

$$K_k = P_{k|k-1}H^\top S_k^{-1}, \qquad x_k = x_{k|k-1} + K_k\big(z_k - Hx_{k|k-1}\big), \qquad P_k = (\tag{7}$$

$\forall$ prediction horizon N, solve

$$\min_{u_{k:k+N-1}} \sum_{i=1}^{N} \big\|Cx_{k+i}^{\mathrm{pred}} - y^\star\big\|_{Q_o}^2 + \|u_{k+i-1}\|_{R_u}^2 \tag{8}$$

subject to the controlled platform-target dynamics

$$x_{k+i+1}^{\mathrm{pred}} = A\big(u_{k+i}\big)\, x_{k+i}^{\mathrm{pred}} + B\big(u_{k+i}\big), \qquad u_{k+i} \in \mathcal{U}, \quad (9)$$

execute $u_k^{\star}$, recede, and repeat.

The ML will develop deep learning in $(T_v, T_\theta, T_{\mathrm{app}}, \gamma)$ in raw IQ data, thus, to reduce false-confirm.

Radio frequency; we are defining the if apply enhanced tracking method with enhancing pipeline, multiprocessing each section of the disected image—— (contracting topological optimizations); thee certainty solution is to define passive listening to the space debris, from radio frequency channeling and missing spots and by 1 miles of difference, localizing the correlation we can derive a system that is able to define the co-difference of the...

refined goal, transmitting the signal on the object and receiving the signal back into a splitted section fed into each pipeline, the FPGA have,

ACKNOWLEDGMENT

Thank you to Professor Hao Xin, and Satnogs community on supporting our data training.

REFERENCES

[1] D. Vallado, P. Crawford, R. Hujsak, and T. Kelso, "Revisiting Spacetrack Report #3," *AIAA*, 2006.
[2] M. I. Skolnik, *Introduction to Radar Systems*, 3rd ed. McGraw-Hill, 2001.
[3] B. Jacob, S. Kligys, B. Chen, et al., "Quantization and Training of Neural Networks for Efficient Integer-Arithmetic-Only Inference," *CVPR Workshops*, 2018.
[4] R. Mahler, *Statistical Multisource-Multitarget Information Fusion*. Artech House, 2007.
[5] Y. Bar-Shalom, X. Li, and T. Kirubarajan, *Estimation with Applications to Tracking and Navigation*. Wiley, 2001.